

# Exact quench dynamics of the Floquet quantum East model at the deterministic point

Bruno Bertini, Cecilia De Fazio, Juan P. Garrahan, and Katja Klobas  
*School of Physics and Astronomy, University of Nottingham, Nottingham, NG7 2RD, UK and  
 Centre for the Mathematics and Theoretical Physics of Quantum  
 Non-Equilibrium Systems, University of Nottingham, Nottingham, NG7 2RD, UK*

We study the non-equilibrium dynamics of the Floquet quantum East model (a Trotterized version of the kinetically constrained quantum East spin chain) at its “deterministic point”, where evolution is defined in terms of CNOT permutation gates. We solve exactly the thermalization dynamics for a broad class of initial product states by means of “space evolution”. We prove: (i) the entanglement of a block of spins grows at most at one-half the maximal speed allowed by locality (i.e., half the speed of dual-unitary circuits); (ii) if the block of spins is initially prepared in a classical configuration, speed of entanglement is a quarter of the maximum; (iii) thermalization to the infinite temperature state is reached exactly in a time that scales with the size of the block.

*Introduction.*— Systems with constrained dynamics are of interest in many areas of non-equilibrium physics. Kinetically constrained models (KCMs) [1–3] provide a framework for explaining [4–6] the emergence of slow and heterogeneous dynamics in glasses [7–10], and their study has spurred the development of dynamical large deviation and trajectory ensemble methods [11–13]. Quantum constrained dynamics emerges naturally in systems such as Rydberg atoms under blockade conditions [14–17], leading to questions about slow thermalisation and non-ergodicity in the absence of disorder [18–31].

The simplest setting for implementing kinetic constraints is in lattice systems with discrete dynamics, such as cellular automata [32, 33] or quantum circuits [34]. For such setups it has been possible to obtain many exact results that underpin our understanding of quantum dynamics, including on operator dynamics, information spreading, and thermalisation (see e.g. Refs. [35–66]). Quantum circuits are also vital for experimental simulation of quantum systems and quantum computation, having been used to demonstrate quantum advantage, perform randomised benchmarking, and to study non-equilibrium Floquet dynamics [67–77]. Here we consider this setting to characterise the dynamical effects of kinetic constraints by studying a circuit version of the quantum East model [78–80], itself a quantum generalisation of the classical East model [2]. Using methods similar to those employed for dual-unitary circuits [53, 61], we solve exactly the thermalization dynamics.

*Model setting.*— More specifically, we consider the non-equilibrium dynamics of the Floquet Quantum East model [80] at its deterministic point, which we refer to as “deterministic Floquet quantum East” (DFQE) model. This system can be thought of as a brickwork quantum circuit, see Fig. 1, acting on a chain of  $2L$  qubits and with local gate given by

$$U = \mathbb{1} \otimes \bar{P} + X \otimes P, \quad (1)$$

where  $P = \mathbb{1} - \bar{P} = (\mathbb{1} + Z)/2$  is the projector to the up state  $|1\rangle$  of the qubit (the down state is denoted by  $|0\rangle$ ) and  $\{X, Y, Z\}$  are Pauli matrices [81]. The quantum

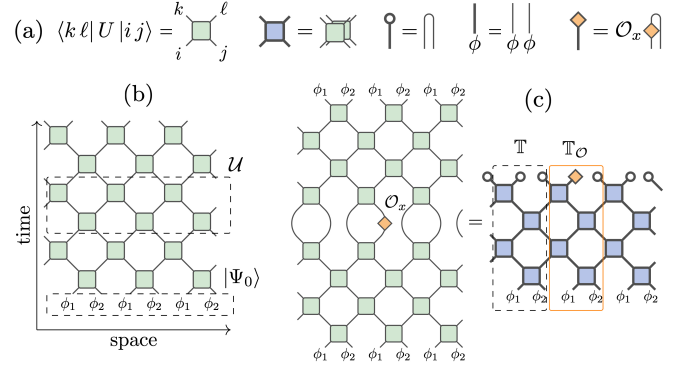


FIG. 1. Deterministic Floquet quantum East model. (a) Diagrammatic representation of the gate Eq. (1). Thick lines correspond to the folded representation of the forward and backward branches. (b) Time evolution of the state as a quantum circuit,  $|\Psi(t)\rangle = U^t |\Psi_0\rangle$ . The dashed boxes indicate the initial state  $|\Psi_0\rangle$  and the evolution operator  $U$  for one time step. (c) One point function of a local operator (l.h.s.) and its folded representation (r.h.s.). The dashed and full boxes outline the space transfer matrices.

circuit with local gate (1) was first studied in Ref. [82] (see also Ref. [83]) and is the quantum counterpart of the classical Floquet East model of Ref. [84]. The gate (1) deterministically implements the constraint that defines both the classical [2, 3] and quantum [78–80] East models, where a site can flip only if its right neighbour is in the up state. The local gate (1) is part of the so called second hierarchy of generalised dual-unitary circuits (DU2) introduced in Ref. [85]. In the jargon of quantum circuits, Eq. (1) is a CNOT (controlled NOT) gate [86], and as such it is a Clifford gate [87, 88]. This implies that there exists a class of initial *stabilizer states* whose dynamics can be efficiently simulated classically. Our discussion, however, is not restricted to this class.

Following a standard quantum quench protocol [89], the system is prepared in an initial state  $|\Psi_0\rangle$ , which we take to be a product state in space, and then let to evolve unitarily as in Fig. 1b. We characterise the ensuing dy-

namics using the so called *space evolution* approach (also known as folding algorithm) [90] (see also Refs. [91–95]). This can be used to characterise the evolution of general local observables [53, 56, 57, 96], quantum information [58, 60, 97–102], and even spectral properties [44, 46–48, 51, 52], but is most easily explained by considering the one-point function of an operator,  $\mathcal{O}_x$ , acting on a single qubit. We represent this via a tensor-network diagram and fold on the portions of the network representing forward and backward evolution, see Fig. 1c, and contract the network horizontally (in space rather than time). Namely, we write the one-point function using the space transfer matrices  $\mathbb{T}$  and  $\mathbb{T}_\mathcal{O}$ , defined in Fig. 1c, as

$$\langle \Psi(t) | \mathcal{O}_x | \Psi(t) \rangle = \text{tr} [\mathbb{T}_\mathcal{O} \mathbb{T}^{L-1}]. \quad (2)$$

Note that the transfer matrices appearing in this expressions act on the vertical folded lattice, i.e., they act on the Hilbert space  $\mathcal{H}_t = \mathbb{C}^{4^{\otimes 2t}}$ , and for simplicity we assumed the initial state to be two-site shift invariant. This latter assumption is not necessary for our analysis and will be explicitly lifted in the second part of this work.

Because of unitarity and locality of the interactions the transfer matrix  $\mathbb{T}$  has a very simple spectrum: its only eigenvalues are 1 and 0 [57, 99]. The transfer matrix itself is *not* rank one, since the eigenvalue zero has generically a non-trivial Jordan structure. However, the size of its Jordan blocks are bounded by  $2t$ , which implies that  $\mathbb{T}^{2t}$  is rank one. It can be written as  $\mathbb{T}^{2t} = |R\rangle\langle L|$ , where  $|R\rangle$  and  $|L\rangle$  are the right and left fixed points of  $\mathbb{T}$  [103]. In other words, for  $L \geq 2t$  the one-point function of interest is fully specified the fixed points. In particular we have

$$\lim_{L \rightarrow \infty} \langle \Psi(t) | \mathcal{O}_x | \Psi(t) \rangle = \langle L | \mathbb{T}_\mathcal{O} | R \rangle. \quad (3)$$

This expression suggests an interesting physical interpretation of the fixed points: they are the mathematical objects encoding the influence of the rest of the system on the subsystem where  $\mathcal{O}$  acts. For this reason they are also referred-to as *influence matrices* [96].

Equation (3) might seem to be a drastic simplification of Eq. (2), as it replaces a complicated matrix product with a matrix element between two fixed points. This form offers practical advantage only when the influence matrices can be computed efficiently, e.g., when they can be represented by matrix product states with low bond dimension. This is not possible in general: for generic systems and initial states, influence matrices have volume law entanglement in time [104]. Some systems, however, avoid this general rule. These includes a class of chaotic dual-unitary circuits [61] evolving from a family of compatible initial states [53], and evolution from compatible states in the Rule 54 quantum cellular automaton [56, 57]. In fact, Ref. [105] argued that in the presence of integrability every low entanglement initial state should generate low entangled influence matrices. Here we show that also the non-integrable DFQE admits

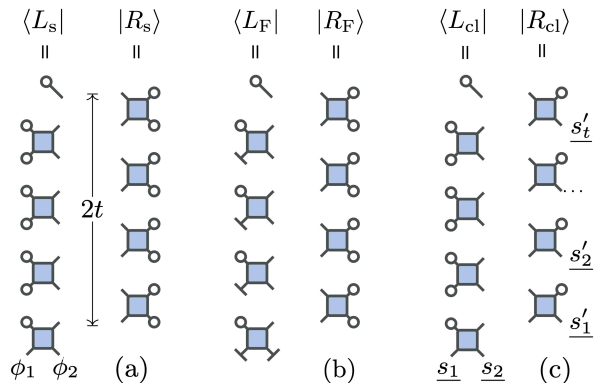


FIG. 2. Fixed points of space transfer matrices. (a) Initial states  $|\phi_{1,2}\rangle$  fulfilling Eq. (5). (b) Flat initial states,  $|\phi_{1,2}\rangle = |-\rangle$ . (c) Classical initial states, in the notation of Eq. (8), where  $s'_1 \equiv s_1 + s_2 \pmod{2}$ ,  $s'_2 = s_2$ , and  $s'_{t'} \equiv s'_{t'-1} + s'_{t'-2} \pmod{2}$  for  $2 < t' \leq t$  (see [106] for details).

*solvable* initial states generating analytically tractable influence matrices. We find *three* distinct families of initial states with influence matrices in dimer-product form, i.e., entangling together only pairs of sites along time. We then use this result to study the exact quench dynamics of a block of spins when the rest of the system is prepared in a solvable state. We show that, regardless of the initial state, the block relaxes to the infinite temperature state in a finite number of time steps. Moreover, we provide an exact description of the full entanglement dynamics if the block is initially prepared in a solvable state.

*Exact Fixed Points.*— We begin by observing that  $U$  in Eq. (1), see Fig. 1, obeys the local relations

$$\begin{aligned} \begin{array}{c} \text{---} \\ \diagdown \\ \text{---} \\ \diagup \\ \text{---} \end{array} &= \begin{array}{c} \text{---} \\ \text{---} \\ \text{---} \end{array}, & \begin{array}{c} \text{---} \\ \diagup \\ \text{---} \\ \diagdown \\ \text{---} \end{array} &= \begin{array}{c} \text{---} \\ \text{---} \\ \text{---} \end{array}, \end{aligned} \quad (4)$$

which define DU2 circuits [85]. Relations (4) imply [85] that if the initial states of two neighbouring sites fulfil

$$\begin{aligned} \begin{array}{c} \text{---} \\ \diagdown \\ \text{---} \\ \diagup \\ \text{---} \end{array} &= \frac{1}{2} \begin{array}{c} \text{---} \\ \text{---} \\ \text{---} \end{array}, & \begin{array}{c} \text{---} \\ \diagup \\ \text{---} \\ \diagdown \\ \text{---} \end{array} &= \frac{1}{2} \begin{array}{c} \text{---} \\ \text{---} \\ \text{---} \end{array}, \end{aligned} \quad (5)$$

the fixed points of the transfer matrix  $\mathbb{T}$  are of the form given in Fig. 2a. To see this consider  $\langle L_s | \mathbb{T}$ , with  $\langle L_s |$  given in Fig. 2a. Starting from above we apply repeatedly the first of (4) until we remove the leftmost column of gates. We then proceed with removing the second column up to the gate applied on the initial state. The latter can be removed using the first of (5) while the numerical factors combine to give  $\langle L_s | \mathbb{T} = \langle L_s |$ . Analogously, using the right relations of (4) and (5) gives  $\mathbb{T} |R_s\rangle = |R_s\rangle$ . Here and in the following we add the subscript “s” to quantities computed for initial states fulfilling (5).

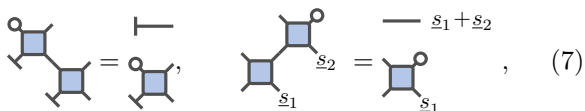
Expressing a general qubit state as  $|\phi\rangle = r e^{i\alpha} |0\rangle + \sqrt{1 - r^2} e^{i\beta} |1\rangle$ , a simple calculation reveals that all states

$|\phi_1\rangle \otimes |\phi_2\rangle$  fulfilling (5) can be parameterised as follows

$$\begin{aligned} 0 &= r_1 r_2 \sqrt{1 - r_1^2} \sqrt{1 - r_2^2} \cos(\alpha_1 - \beta_1) \cos(\alpha_2 - \beta_2), \\ 0 &= \left(r_1^2 - \frac{1}{2}\right) \left(r_2^2 - \frac{1}{2}\right), \end{aligned} \quad (6)$$

where the subscripts 1,2 refer to parameters of  $|\phi_{1,2}\rangle$ . The first equation is fulfilled iff the first of (5) holds while the second iff the second of (5) holds.

A remarkable property of the DFQE is that we do not need to fulfil both these conditions to have simple fixed points. If  $|\phi_{1,2}\rangle$  are both classical configurations  $|0\rangle$  or  $|1\rangle$ , only the first of (5) is fulfilled, however the fixed points display the simple form of Fig. 2b. Similarly, if both  $|\phi_{1,2}\rangle$  are the flat superpositions  $|\phi_1\rangle = |\phi_2\rangle = |-\rangle = (|0\rangle + |1\rangle)/\sqrt{2}$ , only the second of (5) holds but the fixed points take the simple form in Fig. 2c. This is because the local gate fulfils the following relations



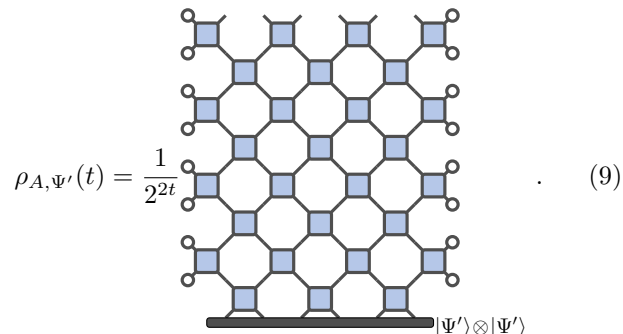
$$\begin{aligned} \text{Diagram 1} &= \text{Diagram 2}, & \text{Diagram 3} &= \text{Diagram 4}, \end{aligned} \quad (7)$$

where we have introduced the diagrams and notation

$$\underline{\perp} = |-\rangle \otimes_r |-\rangle, \quad \underline{s} = |s \bmod 2\rangle \otimes_r |s \bmod 2\rangle, \quad s \in \mathbb{N}_0, \quad (8)$$

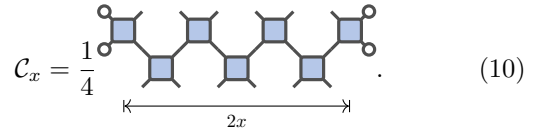
and  $\otimes_r$  indicates that the tensor product is between the states of the same site in the forward and backward branches, see Fig. 1a. The simplification mechanism is very similar to the one discussed after Eq. (5) and we refer the reader to the Supplemental Material [106]. In the following we add the subscripts ‘‘cl’’ and ‘‘F’’ to quantities computed respectively for initial states that are classical configurations and flat superpositions of them [107].

*Subsystem Dynamics.*— The exact expressions for the fixed points in Fig. 2 represent our first main result. To illustrate their power, we use them to determine the relaxation time of a block of  $2\ell$  qubits in a region denoted by  $A$ . In particular, we focus on the quench from the state  $|\Psi_0\rangle = (|\phi_1\rangle \otimes |\phi_2\rangle)^{\otimes L-\ell} \otimes |\Psi'\rangle$ , where  $|\phi_1\rangle \otimes |\phi_2\rangle$  are solvable states (5) and  $|\Psi'\rangle$  is arbitrary [108]. Using the exact expressions in Fig. 2a we find that the reduced density matrix at time  $t$  can be simplified as follows



$$\rho_{A,\Psi'}(t) = \frac{1}{2^{2t}} \text{Diagram} \quad (9)$$

Note how Eq. (9) does not contain explicitly the environment ( $\bar{A}$ , the complement of  $A$ ): its effect is encoded in the boundaries of the time-evolution operator of  $A$ . In other words, the superoperator formed by two subsequent horizontal layers of the tensor network in Eq. (9),



$$\mathcal{C}_x = \frac{1}{4} \text{Diagram} \quad (10)$$

retains information on  $\bar{A}$  only through its depolarising boundaries. In general, tracing out part of a unitarily evolving system gives rise to non-Markovian dissipative evolution on the subsystem [109]. In contrast, for the case of the DFQE the evolution of the subsystem is Markovian and the superoperator  $\mathcal{C}_x$  is a time-local quantum map. Equation (9) represents a drastic simplification: the dynamics of a block of  $2\ell$  spins can be fully determined by diagonalising a  $4^{2\ell} \times 4^{2\ell}$  matrix, which can be done analytically for small  $\ell$  and numerically larger  $\ell$ . Moreover, one can use Eq. (9) to show [106] that  $\rho_A(t) = \mathbb{1}/2^{2\ell}$  for any  $t \geq 2\ell$ , so that the subsystem reaches the maximal entropy state in a *finite* number of steps. This result contrasts with what happens in generic systems, where the presence of exponential corrections means that the stationary state is only reached exactly at infinite time. An analogous situation to the one here is found in dual-unitary circuits [49], with an important difference: in the DFQE the number of steps to approach stationarity is twice larger than for dual-unitaries.

*Entanglement.*— Using the above properties we can compute the growth of entanglement from various homogeneous and inhomogeneous initial states. For concreteness we consider a system that is prepared in a solvable state everywhere, except for a finite subsystem  $A$  of length  $\ell = |A|$ . At some later time  $t$  the Rényi entanglement entropy between  $A$  and the rest is defined as

$$S_{\Psi'}^{(n)}(t) = \frac{1}{1-n} \text{tr}[\rho_{A,\Psi'}^n(t)], \quad (11)$$

where  $n$  is the Rényi index, and  $\rho_{A,\Psi'}(t)$  is given in Eq. (9). Within  $A$  the system is prepared in one of the classes of solvable states: those fulfilling both Eqs. (5), homogeneous *flat* states, or classical configurations.

The entanglement entropies show different scalings depending on the ratio between the subsystem size  $\ell$ , and time  $t$ . In particular, we expect a simple result in the limit  $t \rightarrow \infty$ , where the entropies saturate at a value extensive in  $\ell$  (see Fig. 3b). In fact, the finite-time relaxation discussed above implies that for *any initial state* in  $A$  and  $t \geq 2\ell$  all Rényi entropies are the same

$$S_{\Psi'}^{(n)}(t) \Big|_{t \geq 2\ell} = 2\ell \ln 2. \quad (12)$$

For times that are shorter than  $2\ell$ , there are no immediate simplifications at the level of the single reduced

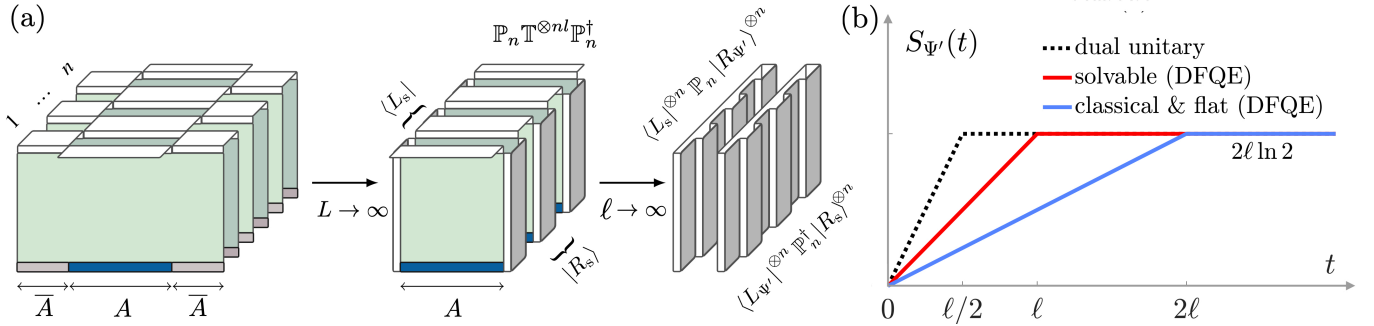


FIG. 3. Rényi entropies and entanglement dynamics. (a) Diagrammatic representation of  $\text{tr}[\rho_A^n]$  for  $n = 3$ . (b) Comparison of entanglement growth between DFQE model (solid lines) and dual-unitary circuits (dashed line). For the DFQE model, the system  $A$  of length  $\ell \ll L$  is initially prepared in a solvable state  $|\Psi'\rangle$  fulfilling (5) and (18) (red line), or one of (5) and one of (7) (blue line). For  $t > 2\ell$  all curves reach the infinite-temperature value  $2\ell \ln 2$ .

density matrix, but we need to consider the full trace in Eq. (11). Assuming for definiteness that inside of the subsystem  $A$  the initial state  $\Psi'$  is a product state and is invariant under lattice shifts by an even number of sites, the generalised purity can be compactly expressed in terms of the corresponding space transfer-matrix  $\mathbb{T}$  as

$$\text{tr}[\rho_{A,\Psi'}^n(t)] = \langle L_s |^{\otimes n} \mathbb{P}_n \mathbb{T}^{\otimes n |A|} \mathbb{P}_n^\dagger | R_s \rangle^{\otimes n}, \quad (13)$$

where  $\mathbb{P}_n$  is an operator that implements the permutation of  $n$  copies, see Fig. 3a. This expression suggests another conceptually simple regime: the “early time” regime where  $t$  is fixed and  $|A|$  is large. In this regime Eq. (13) is written in terms of a large power of a finite matrix expressible in terms of a fixed point: whenever  $t < \ell/2$  the powers of the transfer matrix factorize

$$\mathbb{T}^x |_{x>2t} = |R_{\Psi'}\rangle \langle L_{\Psi'}|, \quad (14)$$

and (13) reduces to a product of two matrix elements,

$$\text{tr}[\rho_{A,\Psi'}^n(t)] = \langle L_s |^{\otimes n} \mathbb{P}_n | R_{\Psi'} \rangle^{\otimes n} \langle L_{\Psi'} |^{\otimes n} \mathbb{P}_n^\dagger | R_s \rangle^{\otimes n}. \quad (15)$$

With the specific form of fixed points, Fig. 2, we can evaluate these overlaps and obtain for the three classes [106]

$$\begin{aligned} S_s^{(n)}(t)|_{2t < \ell} &= 2t \ln 2, \\ S_{\text{cl}}^{(n)}(t)|_{2t < \ell} &= S_F^{(n)}(t)|_{t < \ell} = t \ln 2. \end{aligned} \quad (16)$$

Interestingly, we see that the entanglement entropies all grow with the same slope. Moreover, for classical configurations and their flat superposition this slope is reduced by 2: this is an explicit example of the initial-state dependence of the entanglement velocity. Note that for the flat superposition the range of validity of the early time expression is larger ( $t < \ell$  rather than  $2t < \ell$ ) due to the flat state being locally invariant under the dynamics.

The hardest regime to access is the intermediate-time regime  $\ell/2 < t < 2\ell$ . In this case Eq. (13) does not directly factorise, and cannot be determined only knowing

the fixed points. Remarkably, and in contrast to other known solvable examples [56, 58], Eq. (13) can be evaluated also in this regime for the three cases considered here. This leads to a complete description of the entanglement dynamics so far only attained for dual-unitary circuits [53, 61]. In particular, when the subsystem is prepared in a classical configuration, or the flat state, the partition sum (13) evaluates to  $2^{(1-n)t}$  for all  $t$  in the intermediate regime, i.e.,  $\ell/2 < t < 2\ell$ . This gives [106]

$$S_{\text{cl}}^{(n)}(t) = S_F^{(n)}(t) = \min(t, 2\ell) \ln 2. \quad (17)$$

Instead, if the subsystem is prepared in a *solvable* state that additionally satisfies

$$\begin{aligned} \begin{array}{c} \text{---} \\ \diagdown \quad \diagup \\ \square \\ \diagup \quad \diagdown \\ \text{---} \end{array} &= \begin{array}{c} \text{---} \\ \diagdown \quad \diagup \\ \square \\ \diagup \quad \diagdown \\ \text{---} \end{array}, & \text{---} &= \begin{bmatrix} 1 & 0 & 0 & 0 \\ 0 & 0 & 0 & 0 \\ 0 & 0 & 0 & 0 \\ 0 & 0 & 0 & 1 \end{bmatrix}, \end{aligned} \quad (18)$$

the stationary state is reached at  $t = \ell$  (rather than  $2\ell$ ), and for  $\ell/2 < t < \ell$  Eq. (13) gives  $2^{2t(1-n)}$ . This implies

$$S_s(t) = \min(2t, 2\ell) \ln 2. \quad (19)$$

An interesting question is whether this surprising result can be ascribed to a general property of the initial states. While the DFQE is a Clifford circuit the above is not a consequence of initial states being stabilizer states: even though classical configurations and the flat state are stabilizers, the solvable states fulfilling Eqs. (5) and (18) are generically not. As shown in [106], the exact results in Eqs. (17) and (19) rely on three different “microscopic mechanisms” of simplifications that combine properties of the initial states and the time-evolution. The overall effect, however, is similar in the three cases: the microscopic simplifications decouple the entanglement production at the two boundaries between  $A$  and  $\bar{A}$ . This allows to treat the problem as if it were always in the early time regime. Importantly, Eq. (18) is a necessary requirement



for this to happen: finite-time numerics show that for solvable states that do not satisfy that condition the entanglement entropy deviates from (19) at intermediate times.

*Conclusions.* — We have solved exactly the entanglement dynamics of the deterministic Floquet quantum East model, a quantum circuit defined in terms of local CNOT gates that implement the same kinetic constraint as the East model [2, 78]. To our knowledge, these are the first exact results for entangling dynamics in an interacting non-integrable circuit beyond those in the dual-unitary class. The simplicity of the DFQE model allows its dynamics to be solved in the large size limit for a broad class of initial product states that extends beyond Clifford stabilizers, exploiting the techniques of propagation-in-space. One can think of many avenues for future research. An immediate one is to characterise exactly operator spreading by extending the results of Ref. [110] on the butterfly velocity of DU2 circuits to determine the full profile of out-of-time-ordered correlators. Other directions include studying the effect of local measurements on entanglement at the level of quantum trajectories [62, 63, 111, 112] and the quantification of dynamical fluctuations as is done in the classical Floquet East [84].

We acknowledge financial support from the Royal Society through the University Research Fellowship No. 201101 (B. B.), from EPSRC Grant No. EP/V031201/1 (C. D. F. and J. P. G.), and from The Leverhulme Trust through the Early Career Fellowship No. ECF-2022-324 (K. K.). B. B. and K. K. warmly acknowledge the hospitality of the Simons Center for Geometry and Physics during the program “Fluctuations, Entanglements, and Chaos: Exact Results” where this work was completed.

- 
- [1] G. H. Fredrickson and H. C. Andersen, *Phys. Rev. Lett.* **53**, 1244 (1984).
- [2] J. Jäckle and S. Eisinger, *Z. Phys. B* **84**, 115 (1991).
- [3] F. Ritort and P. Sollich, *Adv. Phys.* **52**, 219 (2003).
- [4] J. P. Garrahan and D. Chandler, *Phys. Rev. Lett.* **89**, 035704 (2002).
- [5] D. Chandler and J. P. Garrahan, *Annu. Rev. Phys. Chem.* **61**, 191 (2010).
- [6] T. Speck, *J. Stat. Mech.: Theory Exp.* **2019** (8), 084015.
- [7] L. Berthier and G. Biroli, *Rev. Mod. Phys.* **83**, 587 (2011).
- [8] G. Biroli and J. P. Garrahan, *J. Chem. Phys.* **138**, 12A301 (2013).
- [9] J. P. Garrahan, *Physica A* **504**, 130 (2018).
- [10] M. R. Hasyim and K. K. Mandadapu, [arXiv:2310.06584](https://arxiv.org/abs/2310.06584) (2023).
- [11] H. Touchette, *Phys. Rep.* **478**, 1 (2009).
- [12] H. Touchette, *Physica A* **504**, 5 (2018).
- [13] R. L. Jack, *Eur. Phys. J. B* **93**, 74 (2020).
- [14] I. Lesanovsky, *Phys. Rev. Lett.* **106**, 025301 (2011).
- [15] H. Bernien, S. Schwartz, A. Keesling, H. Levine, A. Omran, H. Pichler, S. Choi, A. S. Zibrov, M. Endres, M. Greiner, *et al.*, *Nature* **551**, 579 (2017).
- [16] A. Browaeys and T. Lahaye, *Nature Phys.* **16**, 132 (2020).
- [17] D. Bluvstein, A. Omran, H. Levine, A. Keesling, G. Semeghini, S. Ebadi, T. T. Wang, A. A. Michailidis, N. Maskara, W. W. Ho, S. Choi, M. Serbyn, M. Greiner, V. Vuletić, and M. D. Lukin, *Science* **371**, 1355 (2021).
- [18] C. J. Turner, A. A. Michailidis, D. A. Abanin, M. Serbyn, and Z. Papić, *Nature Phys.* **14**, 745 (2018).
- [19] W. W. Ho, S. Choi, H. Pichler, and M. D. Lukin, *Phys. Rev. Lett.* **122**, 040603 (2019).
- [20] S. Choi, C. J. Turner, H. Pichler, W. W. Ho, A. A. Michailidis, Z. Papić, M. Serbyn, M. D. Lukin, and D. A. Abanin, *Phys. Rev. Lett.* **122**, 220603 (2019).
- [21] P. Sala, T. Rakovszky, R. Verresen, M. Knap, and F. Pollmann, *Phys. Rev. X* **10**, 011047 (2020).
- [22] L. Zadnik and M. Fagotti, *SciPost Phys. Core* **4**, 010 (2021).
- [23] L. Zadnik, K. Bidzhiev, and M. Fagotti, *SciPost Phys.* **10**, 099 (2021).
- [24] B. Pozsgay, T. Gombor, A. Hutsalyuk, Y. Jiang, L. Pristiyák, and E. Vernier, *Phys. Rev. E* **104**, 044106 (2021).
- [25] H. Singh, B. A. Ware, R. Vasseur, and A. J. Friedman, *Phys. Rev. Lett.* **127**, 230602 (2021).
- [26] M. Serbyn, D. A. Abanin, and Z. Papić, *Nat. Phys.* **17**, 675 (2021).
- [27] S. Moudgalya, B. A. Bernevig, and N. Regnault, *Rep. Prog. Phys.* **85**, 086501 (2022).
- [28] H. Singh, R. Vasseur, and S. Gopalakrishnan, *Phys. Rev. Lett.* **130**, 046001 (2023).
- [29] S. Gopalakrishnan, A. Morningstar, R. Vasseur, and V. Khemani, Distinct universality classes of diffusive transport from full counting statistics (2022), [arXiv:2203.09526](https://arxiv.org/abs/2203.09526).
- [30] M. Ljubotina, J.-Y. Desaulles, M. Serbyn, and Z. Papić, *Phys. Rev. X* **13**, 011033 (2023).
- [31] P. Brighi, M. Ljubotina, and M. Serbyn, *SciPost Phys.* **15**, 093 (2023).
- [32] S. Wolfram, *Rev. Mod. Phys.* **55**, 601 (1983).
- [33] A. Bobenko, M. Bordemann, C. Gunn, and U. Pinkall, *Commun. Math. Phys.* **158**, 127 (1993).
- [34] T. J. Osborne, *Phys. Rev. Lett.* **97**, 157202 (2006).
- [35] A. Nahum, J. Ruhman, S. Vijay, and J. Haah, *Phys. Rev. X* **7**, 031016 (2017).
- [36] C. W. von Keyserlingk, T. Rakovszky, F. Pollmann, and S. L. Sondhi, *Phys. Rev. X* **8**, 021013 (2018).
- [37] A. Chan, A. De Luca, and J. T. Chalker, *Phys. Rev. X* **8**, 041019 (2018).
- [38] V. Khemani, A. Vishwanath, and D. A. Huse, *Phys. Rev. X* **8**, 031057 (2018).
- [39] T. Rakovszky, F. Pollmann, and C. W. von Keyserlingk, *Phys. Rev. X* **8**, 031058 (2018).
- [40] T. Zhou and A. Nahum, *Phys. Rev. X* **10**, 031066 (2020).
- [41] I. Reid and B. Bertini, *Phys. Rev. B* **104**, 014301 (2021).
- [42] H. Wang and T. Zhou, *J. High Energy Phys.* **2019** (12), 1.
- [43] A. J. Friedman, A. Chan, A. De Luca, and J. T. Chalker, *Phys. Rev. Lett.* **123**, 210603 (2019).
- [44] B. Bertini, P. Kos, and T. Prosen, *Phys. Rev. Lett.* **121**,

- 264101 (2018).
- [45] A. Chan, A. De Luca, and J. T. Chalker, *Phys. Rev. Lett.* **121**, 060601 (2018).
- [46] A. Flack, B. Bertini, and T. Prosen, *Phys. Rev. Research* **2**, 043403 (2020).
- [47] B. Bertini, P. Kos, and T. Prosen, *Commun. Math. Phys.* **387**, 597 (2021).
- [48] F. Fritzsche and T. Prosen, *Phys. Rev. E* **103**, 062133 (2021).
- [49] P. Kos, T. Prosen, and B. Bertini, *Phys. Rev. B* **104**, 214303 (2021).
- [50] B. Bertini, P. Kos, and T. Prosen, *Phys. Rev. B* **105**, 165142 (2022).
- [51] S. J. Garratt and J. T. Chalker, *Phys. Rev. Lett.* **127**, 026802 (2021).
- [52] S. J. Garratt and J. T. Chalker, *Phys. Rev. X* **11**, 021051 (2021).
- [53] L. Piroli, B. Bertini, J. I. Cirac, and T. Prosen, *Phys. Rev. B* **101**, 094304 (2020).
- [54] P. W. Claeys and A. Lamacraft, *Phys. Rev. Lett.* **126**, 100603 (2021).
- [55] R. Suzuki, K. Mitarai, and K. Fujii, *Quantum* **6**, 631 (2022).
- [56] K. Klobas, B. Bertini, and L. Piroli, *Phys. Rev. Lett.* **126**, 160602 (2021).
- [57] K. Klobas and B. Bertini, *SciPost Phys.* **11**, 106 (2021).
- [58] K. Klobas and B. Bertini, *SciPost Phys.* **11**, 107 (2021).
- [59] A. Nahum, S. Vijay, and J. Haah, *Phys. Rev. X* **8**, 021014 (2018).
- [60] B. Bertini, P. Kos, and T. Prosen, *Phys. Rev. X* **9**, 021033 (2019).
- [61] B. Bertini, P. Kos, and T. Prosen, *Phys. Rev. Lett.* **123**, 210601 (2019).
- [62] Y. Li, X. Chen, and M. P. A. Fisher, *Phys. Rev. B* **100**, 134306 (2019).
- [63] B. Skinner, J. Ruhman, and A. Nahum, *Phys. Rev. X* **9**, 031009 (2019).
- [64] T. Rakovszky, F. Pollmann, and C. W. von Keyserlingk, *Phys. Rev. Lett.* **122**, 250602 (2019).
- [65] A. Zabalo, M. J. Gullans, J. H. Wilson, S. Gopalakrishnan, D. A. Huse, and J. H. Pixley, *Phys. Rev. B* **101**, 060301(R) (2020).
- [66] P. W. Claeys and A. Lamacraft, *Phys. Rev. Research* **2**, 033032 (2020).
- [67] T. Brydges, A. Elben, P. Jurcevic, B. Vermersch, C. Maier, B. P. Lanyon, P. Zoller, R. Blatt, and C. F. Roos, *Science* **364**, 260 (2019).
- [68] A. Elben, J. Yu, G. Zhu, M. Hafezi, F. Pollmann, P. Zoller, and B. Vermersch, *Sci. Adv.* **6**, eaaz3666 (2020).
- [69] A. Elben, B. Vermersch, M. Dalmonte, J. I. Cirac, and P. Zoller, *Phys. Rev. Lett.* **120**, 050406 (2018).
- [70] H. Pichler, G. Zhu, A. Seif, P. Zoller, and M. Hafezi, *Phys. Rev. X* **6**, 041033 (2016).
- [71] B. Vermersch, A. Elben, L. M. Sieberer, N. Y. Yao, and P. Zoller, *Phys. Rev. X* **9**, 021061 (2019).
- [72] B. Vermersch, A. Elben, M. Dalmonte, J. I. Cirac, and P. Zoller, *Phys. Rev. A* **97**, 023604 (2018).
- [73] S. Aaronson, [arXiv:1711.01053](https://arxiv.org/abs/1711.01053) (2018).
- [74] H.-Y. Huang, R. Kueng, and J. Preskill, *Nat. Phys.* **16**, 1050 (2020).
- [75] M. Ohliger, V. Nesme, and J. Eisert, *New J. Phys.* **15**, 015024 (2013).
- [76] N. Keenan, N. F. Robertson, T. Murphy, S. Zhuk, and J. Goold, *Npj Quantum Inf.* **9**, 72 (2023).
- [77] A. Morvan, T. Andersen, X. Mi, C. Neill, A. Petukhov, K. Kechedzhi, D. Abanin, A. Michailidis, R. Acharya, F. Arute, *et al.*, *Nature* **612**, 240 (2022).
- [78] M. van Horssen, E. Levi, and J. P. Garrahan, *Phys. Rev. B* **92**, 100305 (2015).
- [79] N. Pancotti, G. Giudice, J. I. Cirac, J. P. Garrahan, and M. C. Bañuls, *Phys. Rev. X* **10**, 021051 (2020).
- [80] B. Bertini, P. Kos, and T. c. v. Prosen, *Phys. Rev. Lett.* **132**, 080401 (2024).
- [81] This gate can be recovered from the gate in Eq. (5) of Ref. [80] by performing a space inversion and setting  $a = 1$  and  $\tau = \pi/2$ .
- [82] S. Gopalakrishnan and B. Zakirov, *Quantum Sci. Technol.* **3**, 044004 (2018).
- [83] D. Berenstein and J. Zhao, [arXiv:2102.05745](https://arxiv.org/abs/2102.05745) (2021).
- [84] K. Klobas, C. De Fazio, and J. P. Garrahan, [arXiv:2305.07423](https://arxiv.org/abs/2305.07423) (2023).
- [85] X.-H. Yu, Z. Wang, and P. Kos, *Quantum* **8**, 1260 (2024).
- [86] M. A. Nielsen and I. L. Chuang, *Quantum computation and quantum information* (Cambridge university press, 2010).
- [87] D. Gottesman, [arXiv:quant-ph/9807006](https://arxiv.org/abs/quant-ph/9807006) (1998).
- [88] J. Gütschow, S. Uphoff, R. F. Werner, and Z. Zimborás, *J. Math. Phys.* **51**, 015203 (2010).
- [89] P. Calabrese and J. Cardy, *Phys. Rev. Lett.* **96**, 136801 (2006).
- [90] M. C. Bañuls, M. B. Hastings, F. Verstraete, and J. I. Cirac, *Phys. Rev. Lett.* **102**, 240603 (2009).
- [91] A. Müller-Hermes, J. I. Cirac, and M. C. Bañuls, *New J. Phys.* **14**, 075003 (2012).
- [92] M. B. Hastings and R. Mahajan, *Phys. Rev. A* **91**, 032306 (2015).
- [93] M. Sonner, A. Leroose, and D. A. Abanin, *Phys. Rev. B* **105**, L020203 (2022).
- [94] M. Frías-Pérez and M. C. Bañuls, *Phys. Rev. B* **106**, 115117 (2022).
- [95] A. Leroose, M. Sonner, and D. A. Abanin, *Phys. Rev. B* **107**, L060305 (2023).
- [96] A. Leroose, M. Sonner, and D. A. Abanin, *Phys. Rev. X* **11**, 021040 (2021).
- [97] M. Ippoliti and V. Khemani, *Phys. Rev. Lett.* **126**, 060501 (2021).
- [98] M. Ippoliti, T. Rakovszky, and V. Khemani, *Phys. Rev. X* **12**, 011045 (2022).
- [99] B. Bertini, K. Klobas, and T.-C. Lu, *Phys. Rev. Lett.* **129**, 140503 (2022).
- [100] B. Bertini, K. Klobas, V. Alba, G. Lagnese, and P. Calabrese, *Phys. Rev. X* **12**, 031016 (2022).
- [101] B. Bertini, P. Calabrese, M. Collura, K. Klobas, and C. Rylands, *Phys. Rev. Lett.* **131**, 140401 (2023).
- [102] B. Bertini, K. Klobas, M. Collura, P. Calabrese, and C. Rylands, [arXiv:2306.12404](https://arxiv.org/abs/2306.12404) (2023).
- [103] We choose the normalisation such that  $\langle R|L \rangle = 1$ .
- [104] A. Foligno, T. Zhou, and B. Bertini, *Phys. Rev. X* **13**, 041008 (2023).
- [105] G. Giudice, G. Giudici, M. Sonner, J. Thoenniss, A. Leroose, D. A. Abanin, and L. Piroli, *Phys. Rev. Lett.* **128**, 220401 (2022).
- [106] See the Supplemental Material.
- [107] Even though the space transfer matrix depends on the initial state, in order to simplify the notation, we will use the same symbol  $\mathbb{T}$  to denote the space transfer matrix



where the normalisation is chosen such that  $\langle L_s | R_s \rangle = 1$ . The left vector indeed satisfies

$$\langle L_s | \mathbb{T} = 2^{-t+1} \begin{array}{c} \text{diag} \\ \text{diag} \\ \text{diag} \\ \text{diag} \\ \text{diag} \\ \phi_1 \quad \phi_2 \quad \phi_1 \quad \phi_2 \end{array} = 2^{-t+2} \begin{array}{c} \text{diag} \\ \text{diag} \\ \text{diag} \\ \text{diag} \\ \text{diag} \\ \phi_1 \quad \phi_2 \quad \phi_1 \quad \phi_2 \end{array} = 2^{-t+2} \begin{array}{c} \text{diag} \\ \text{diag} \\ \text{diag} \\ \text{diag} \\ \text{diag} \\ \phi_1 \quad \phi_2 \quad \phi_1 \quad \phi_2 \end{array} = 2^{-t+1} \begin{array}{c} \text{diag} \\ \text{diag} \\ \text{diag} \\ \text{diag} \\ \text{diag} \\ \phi_1 \quad \phi_2 \end{array} = 2^{-t+1} \begin{array}{c} \text{diag} \\ \text{diag} \\ \text{diag} \\ \text{diag} \\ \text{diag} \\ \phi_1 \quad \phi_2 \end{array} = \langle L_s |, \quad (\text{SM-3})$$

where we start contracting the above tensor network from the top by using

$$\begin{array}{c} \text{diag} \\ \text{diag} \\ \text{diag} \\ \text{diag} \end{array} = 2 \begin{array}{c} \text{diag} \\ \text{diag} \end{array}. \quad (\text{SM-4})$$

The leftmost column is then removed by repeatedly applying the left of (4), and the left of (5) in the end. In the second last equality we further apply the left of (4), to contract the second column.

Similarly, the right vector  $|R_s\rangle$  satisfies:

$$\mathbb{T} |R_s\rangle = 2^{-t} \begin{array}{c} \text{diag} \\ \text{diag} \\ \text{diag} \\ \text{diag} \\ \text{diag} \\ \phi_1 \quad \phi_2 \end{array} = 2^{-t} \begin{array}{c} \text{diag} \\ \text{diag} \\ \text{diag} \\ \text{diag} \\ \text{diag} \\ \phi_1 \quad \phi_2 \end{array} = 2^{-t} 2 \begin{array}{c} \text{diag} \\ \text{diag} \\ \text{diag} \\ \text{diag} \\ \text{diag} \\ \phi_1 \quad \phi_2 \end{array} = 2^{-t} 2 \begin{array}{c} \text{diag} \\ \text{diag} \\ \text{diag} \\ \text{diag} \\ \text{diag} \\ \phi_1 \quad \phi_2 \end{array} = 2^{-t} \begin{array}{c} \text{diag} \\ \text{diag} \\ \text{diag} \\ \text{diag} \\ \text{diag} \\ \phi_1 \quad \phi_2 \end{array} = |R_s\rangle. \quad (\text{SM-5})$$

Above, the first contraction follows from unitarity and produces a factor  $1/2$ . We then contract the rightmost column iterating the right relation in (5). The same for the other column, where we also use the right of (5) to contract the last bit, which cancels out the factor  $1/2$ .

We now consider the states  $|\phi_1\rangle = |\phi_2\rangle = |-\rangle$ . The corresponding (normalised) fixed points are:

$$\langle L_F | = \begin{array}{c} \text{diag} \\ \text{diag} \\ \text{diag} \\ \text{diag} \\ \text{diag} \end{array}, \quad |R_F\rangle = 2^{-t+1} \begin{array}{c} \text{diag} \\ \text{diag} \\ \text{diag} \\ \text{diag} \\ \text{diag} \end{array}. \quad (\text{SM-6})$$



Indeed the left vector satisfies

$$\langle L_F | \mathbb{T} = \text{[Diagram]} = \text{[Diagram]} = \text{[Diagram]} = \text{[Diagram]} = \langle L_F |. \quad (\text{SM-7})$$

In this case, we use the left relation in (7) to contract both the left columns from the bottom to the top. The fact that  $|R_F\rangle$  satisfies  $\mathbb{T}|R_F\rangle = |R_F\rangle$  follows immediately from (SM-5) as the flat states fulfil the same relations used in the previous calculation.

We finally consider classical states i.e.,  $|\phi_1\rangle = |s_1\rangle$  and  $|\phi_2\rangle = |s_2\rangle$ , with  $s_1, s_2 \in \mathbb{Z}_2$ . We have that the corresponding fixed points are:

$$\langle L_{\text{cl}} | = 2^{-t+1} \text{[Diagram]}, \quad |R_{\text{cl}}\rangle = \text{[Diagram]}, \quad (\text{SM-8})$$

where the classical configuration  $\{s'_j\}$  is given as

$$s'_j \equiv s'_{j-1} + s'_{j-2} \pmod{2} \quad \text{for } 2 < j \leq t, \quad s'_2 = s_2, \quad s'_1 \equiv s_1 + s_2 \pmod{2}. \quad (\text{SM-9})$$

In particular  $\{s'_j\}$  is a periodic sequence with period 3. Since classical configurations fulfil the same relations as used in (SM-3), the left vector is the same as in the solvable case,  $\langle L_{\text{cl}} | = \langle L_{\text{s}} |$ . To show that  $|R_{\text{cl}}\rangle$  as introduced above is the right fixed point, however, it requires some additional work. We start by applying the classical transfer matrix to  $|R_{\text{cl}}\rangle$ , without specifying  $s'_j$  (this will be done at the end), and we contract the rightmost column by using the right of (7),

$$\mathbb{T}|R_{\text{cl}}\rangle = \text{[Diagram]} = \text{[Diagram]} = \text{[Diagram]}, \quad (\text{SM-10})$$

where (7) implies

$$s_j'' \equiv \sum_{k=1}^{j-1} s_k' + s_2 \pmod{2}. \quad (\text{SM-11})$$

Repeating the same steps again we obtain

$$\mathbb{T}|R_{\text{cl}}\rangle = \begin{array}{c} \text{Diagram 1} \\ \text{Diagram 2} \\ \text{Diagram 3} \\ \text{Diagram 4} \\ \text{Diagram 5} \\ \text{Diagram 6} \end{array} = \begin{array}{c} \text{Diagram 7} \\ \text{Diagram 8} \\ \text{Diagram 9} \\ \text{Diagram 10} \\ \text{Diagram 11} \\ \text{Diagram 12} \end{array}, \quad s_1''' \equiv s_1 + s_2 \pmod{2}, \quad s_j''' \equiv s_1''' + \sum_{k=2}^j s_k'' \pmod{2}. \quad (\text{SM-12})$$

Simplifying this we get

$$s_{2j}''' \equiv s_1 + \sum_{k=1}^j s'_{2k-1} \pmod{2}, \quad s_{2j-1}''' \equiv s_1 + s_2 + \sum_{k=1}^{j-1} s'_{2k} \pmod{2}. \quad (\text{SM-13})$$

Imposing now the fixed point condition (i.e.,  $s_j''' = s_j'$ ) on (SM-13), we finally obtain the form in (SM-9).

## ENTANGLEMENT ENTROPY

### Early-time regime

Using the explicit form of fixed-points as given in Fig. 2, we can express the factors appearing in the main-text Eq. (15) as a  $2n \times 2t$  tensor network

$$\langle L_{\Psi_2} |^{\otimes n} \mathbb{P}_n | R_{\Psi_1} \rangle^{\otimes n} = \langle L_{\Psi_2} |^{\otimes n} \mathbb{P}_n^\dagger | R_{\Psi_1} \rangle^{\otimes n} = \begin{array}{c} \text{Diagram 1} \\ \text{Diagram 2} \\ \text{Diagram 3} \\ \text{Diagram 4} \end{array}, \quad (\text{SM-14})$$

where the subscripts refer to fixed-points of different initial states. The tensors  $A$  and  $B$  are given as,

$$\begin{aligned} \boxed{A_s} &= \boxed{A_F} = \frac{1}{2} \left( + \frac{1}{2} \right) \otimes \otimes, & \otimes &= \begin{bmatrix} 0 & 1 \\ 1 & 0 \end{bmatrix}, & \boxed{A_3^{(j)}} &= \delta_{b_j, 0} \left( + \delta_{b_j, 1} \right) \otimes \otimes, \\ \boxed{B_s} &= \boxed{B_{\text{cl}}} = \times, & \boxed{B_F} &= \text{ ) } ( \end{aligned} \quad (\text{SM-15})$$

Here s, F, and cl respectively stand for “solvable”, “flat”, and “classical”. Moreover, we note that in the case of the classical configuration  $A$  depends on the precise value of  $b_j$  at the time-step  $j$ . The initial-state tensors  $C$  are given as,

$$\boxed{C_s} = \frac{1}{2} \curvearrowright + \boxed{D}, \quad \boxed{C_{cl}} = \curvearrowright_{s_2 s_2}, \quad \boxed{C_F} = \curvearrowright \curvearrowleft. \quad (\text{SM-16})$$

Here the precise form of  $D$  depends on the choice of the solvable initial state, but it always satisfies

$$\boxed{D} = \boxed{D}^{\otimes} = 0. \quad (\text{SM-17})$$

The tensor-network in (SM-14) can be easily contracted in the vertical direction by defining the transfer matrix  $\mathbb{M}_1^{(n)}$  in the  $\mathbb{C}^{\otimes 2n}$  space, and the corresponding boundary vectors  $\langle t^{(n)} |, |b_{1,2}^{(n)}\rangle$  (grey boxes in (SM-14)). We note that  $\langle t^{(n)} |$  is a (left) eigenvector of  $\mathbb{M}_{1,2}^{(n)}$  for any choice of the superscripts 1, 2 (and — in the case of the classical configuration — independent of value  $b_j$ )

$$\begin{aligned} \langle t_s^{(n)} | \mathbb{M}_{s,s}^{(n)} &= 2^{1-n} \langle t_s^{(n)} |, & \langle t_s^{(n)} | \mathbb{M}_{s,cl}^{(n)} &= 2^{1-n} \langle t_s^{(n)} |, & \langle t_s^{(n)} | \mathbb{M}_{s,F}^{(n)} &= \langle t_s^{(n)} |, \\ \langle t_{cl}^{(n)} | \mathbb{M}_{cl,s}^{(n)} &= \langle t_{cl}^{(n)} |, & \langle t_{cl}^{(n)} | \mathbb{M}_{cl,cl}^{(n)} &= \langle t_{cl}^{(n)} |, & \langle t_{cl}^{(n)} | \mathbb{M}_{cl,F}^{(n)} &= \langle t_{cl}^{(n)} |, \\ \langle t_F^{(n)} | \mathbb{M}_{F,s}^{(n)} &= 2^{1-n} \langle t_F^{(n)} |, & \langle t_F^{(n)} | \mathbb{M}_{F,cl}^{(n)} &= 2^{1-n} \langle t_F^{(n)} |, & \langle t_F^{(n)} | \mathbb{M}_{F,F}^{(n)} &= \langle t_F^{(n)} |. \end{aligned} \quad (\text{SM-18})$$

To obtain the matrix elements (SM-14) the only thing left to evaluate are the overlaps  $\langle t_1^{(n)} | b_2^{(n)} \rangle$ ,

$$\begin{aligned} \langle t_s^{(n)} | b_s^{(n)} \rangle &= 2^{1-n}, & \langle t_s^{(n)} | b_{cl}^{(n)} \rangle &= 2^{1-n}, & \langle t_s^{(n)} | b_F^{(n)} \rangle &= 1, \\ \langle t_{cl}^{(n)} | b_s^{(n)} \rangle &= 1, & \langle t_{cl}^{(n)} | b_{cl}^{(n)} \rangle &= 1, & \langle t_{cl}^{(n)} | b_F^{(n)} \rangle &= 1, \\ \langle t_F^{(n)} | b_s^{(n)} \rangle &= 2^{1-n}, & \langle t_F^{(n)} | b_{cl}^{(n)} \rangle &= 2^{1-n}, & \langle t_F^{(n)} | b_F^{(n)} \rangle &= 1, \end{aligned} \quad (\text{SM-19})$$

which finally give

$$\begin{aligned} \langle L_s |^{\otimes n} \mathbb{P}_n | R_s \rangle^{\otimes n} &= \langle L_s |^{\otimes n} \mathbb{P}_n^\dagger | R_s \rangle^{\otimes n} = 2^{(1-n)t}, \\ \langle L_s |^{\otimes n} \mathbb{P}_n | R_F \rangle^{\otimes n} &= \langle L_{cl} |^{\otimes n} \mathbb{P}_n^\dagger | R_s \rangle^{\otimes n} = 2^{(1-n)t}, \\ \langle L_s |^{\otimes n} \mathbb{P}_n | R_{cl} \rangle^{\otimes n} &= \langle L_F |^{\otimes n} \mathbb{P}_n^\dagger | R_s \rangle^{\otimes n} = 1. \end{aligned} \quad (\text{SM-20})$$

### Late-time regime

When  $t \rightarrow \infty$  we typically expect the finite-subsystem to relax to the stationary state regardless of the initial state. For special initial states considered here, the relaxation happens in *finite* time. To see this, we consider the following transfer matrix, which gives the exact dynamics of a subsystem immersed in the large system of solvable states,

$$C_x = \frac{1}{4} \begin{array}{c} \circ \quad \square \quad \square \quad \square \quad \square \quad \square \quad \circ \\ \diagdown \quad \diagup \quad \diagdown \quad \diagup \quad \diagdown \quad \diagup \\ \square \quad \square \quad \square \quad \square \quad \square \quad \square \\ \diagup \quad \diagdown \quad \diagup \quad \diagdown \quad \diagup \quad \diagdown \\ \circ \quad \square \quad \square \quad \square \quad \square \quad \square \quad \circ \\ \underbrace{\hspace{10em}}_{2x} \end{array}, \quad (\text{SM-21})$$

where the  $x$  denotes the size of the subsystem, which in our convention implies  $2x$  open legs (cf. the label). For concreteness and simplicity we will always consider an *even* number of legs, but with minor modifications the claims

can be applied also to odd numbers. In this case the  $2x$ -th power of the transfer matrix is expressed as,

$$C_x^{2x} = 2^{-4x} \left[ \text{Diagram 1} \right] = 2^{-2x} \left[ \text{Diagram 2} \right], \quad (\text{SM-22})$$

where  $\diamond$  is the projector to the subspace with both legs in the same state,

$$\diamond = \begin{bmatrix} 1 & 0 & 0 & 0 \\ 0 & 0 & 0 & 0 \\ 0 & 0 & 0 & 0 \\ 0 & 0 & 0 & 1 \end{bmatrix}, \quad (\text{SM-23})$$

and the r.h.s. follows from

$$\text{Diagram 1} = 2 \left( \text{Diagram 2} \right), \quad \text{Diagram 2} = \text{Diagram 3}. \quad (\text{SM-24})$$

Now we note that the following holds,

$$\text{Diagram 1} = \text{Diagram 2} = \text{Diagram 3} = \text{Diagram 4}, \quad (\text{SM-25})$$

which allows us to simplify the above tensor-network into

$$C_x^{2x} = 2^{-2x} \left[ \text{Diagram 1} \right] = 2^{-2x} \left[ \text{Diagram 2} \right] = 2^{-2x} \left[ \text{Diagram 3} \right], \quad (\text{SM-26})$$

where the second equality follows from repeated application of (SM-25), together with the 2nd hierarchy condition and (SM-24). To obtain the last equality, we use unitarity together with the invariance of  $\diamond$  under  $\phi$ .

Eq. (SM-26) suggests that application of  $C_x$  of at least  $2x$  times to *any* initial state results in the maximum entropy state. In particular, this means that starting with the system initialized in the solvable state everywhere except possibly inside a finite subsystem  $A$ , the density matrix reduced to the subsystem  $A$  will be after  $2\ell$ ,  $\ell = |A|$ , exactly given by the maximum entropy state,

$$\rho_A(t)|_{t \geq 2\ell} = \frac{1}{2^{2\ell}} \mathbb{1}, \quad \ell = |A|. \quad (\text{SM-27})$$





reduced density matrix is not yet equal to the stationary one, and at the same time the powers of the space transfer matrix do not factorize. The reduced density matrix is in this case given by the following diagram,

(SM-33)

To express traces of powers of the reduced density matrix we can imagine to take many copies (replicas) of the diagram above, and connect the top legs in the staggered way. By introducing dark squares as the notation for  $n$  copies of the folded gate (i.e., each leg now represents  $2n$  qubits), and  $\blacklozenge$ ,  $\blacklozenge$  as symbols for the two different pairings of the  $2n$  legs

(SM-34)

we can express the trace of  $n$ -th power of  $\rho_A(t)$  as

(SM-35)

Now we introduce a  $n$ -generalization of  $\blacklozenge$  as

$$\blacklozenge = \begin{bmatrix} 1 & 0 & 0 & 0 \\ 0 & 0 & 0 & 0 \\ 0 & 0 & 0 & 0 \\ 0 & 0 & 0 & 1 \end{bmatrix}^{\otimes n},$$

(SM-36)

which — analogously to the  $n = 1$  case — satisfies

(SM-37)

Repeatedly applying them — together with the initial-state condition (SM-28), and the unitarity from the top — allows us to rewrite (SM-35) as

$$\text{tr}[\rho_A^n] = 2^{-nt} \left( \begin{array}{c} \square \\ \phi_1 \end{array} \begin{array}{c} \square \\ \phi_2 \end{array} \right)^{\ell-t} \quad (\text{SM-38})$$

To progress from here, we note that the condition (SM-28) is satisfied whenever at least one of  $\phi_1$  and  $\phi_2$  is a classical state, i.e., it is either  $[1, 0]$  or  $[0, 1]$ . Using now

$$\begin{array}{c} \square \\ \underline{s} \end{array} = \frac{1}{2} \begin{array}{c} \square \\ \square \end{array}, \quad \begin{array}{c} \square \\ \phi \end{array} \begin{array}{c} \square \\ \underline{s} \end{array} = \frac{1}{2} \begin{array}{c} \square \\ \phi \end{array} \begin{array}{c} \square \\ \square \end{array}, \quad (\text{SM-39})$$

we find the following generalisation of Eq. (5) of the main text

$$\begin{array}{c} \square \\ \underline{s} \end{array} \begin{array}{c} \square \\ \square \end{array} = 2^{-n} \begin{array}{c} \square \\ \square \end{array} \begin{array}{c} \square \\ \square \end{array} = 2^{-n} \begin{array}{c} \square \\ \square \end{array}, \quad \begin{array}{c} \square \\ \phi \end{array} \begin{array}{c} \square \\ \underline{s} \end{array} = \begin{array}{c} \square \\ \phi \end{array} 2^{-n} \begin{array}{c} \square \\ \square \end{array} \begin{array}{c} \square \\ \underline{s} \end{array}. \quad (\text{SM-40})$$

Here and in the following we denote by  $\underline{s}$  a classical configuration on all the  $2n$  copies. These equations in particular imply

$$\begin{array}{c} \square \\ \phi_1 \end{array} \begin{array}{c} \square \\ \phi_2 \end{array} \begin{array}{c} \square \\ \square \end{array} = 2^{-n} \begin{array}{c} \square \\ \phi_1 \end{array} \begin{array}{c} \square \\ \phi_2 \end{array} \begin{array}{c} \square \\ \square \end{array}. \quad (\text{SM-41})$$

This reduces the triangle in (SM-38) into

$$\text{tr}[\rho_A^n(t)] = 2^{-2tn} \left( \begin{array}{c} \square \\ \phi_1 \end{array} \begin{array}{c} \square \\ \phi_2 \end{array} \right)^t \left( \begin{array}{c} \square \\ \square \end{array} \right)^t. \quad (\text{SM-42})$$

The only thing left to do is to combine all the relevant factors

$$\begin{array}{c} \square \\ \square \end{array} = 2^{n+1}, \quad \begin{array}{c} \square \\ \phi_1 \end{array} \begin{array}{c} \square \\ \phi_2 \end{array} = 2^{-n+1}, \quad (\text{SM-43})$$

where we remark that the second equality holds for all initial states that are both solvable and satisfy (SM-28) (i.e., they are in the subset considered here). This finally gives

$$\text{tr}[\rho_A^n(t)] = 2^{2t(1-n)}. \quad (\text{SM-44})$$

As a final point, we remark that here we never explicitly used translational invariance of the initial state, and pairs  $(\phi_1, \phi_2)$  could be chosen independently for all pairs of sites (as long as the relevant conditions are satisfied) without changing the result.

*Classical subregion in a system prepared in a solvable state*

Let us now consider entanglement entropy between the subsystem  $A$  and the rest, where the rest is prepared in the solvable state, while  $A$  is initialized in a classical configuration. First we treat the regime  $t < \ell < 2t$ , and we denote the classical configuration by  $[s_1, s_2, \dots, s_{2\ell}]$ . Diagrammatically, the trace of powers of the reduced density matrix takes the following form

$$\text{tr}[\rho_A^n(t)] = 2^{-2nt} \cdot \text{Diagram} \quad (\text{SM-45})$$

Using the same simplifications as in the previous section we obtain

$$\text{tr}[\rho_A^n(t)] = 2^{-2tn} \left( \text{Diagram} \right)^t = 2^{t(1-n)}. \quad (\text{SM-46})$$

We now consider the regime  $\frac{t}{2} < \ell < t$  and compute the following

$$\text{tr}[\rho_A^n(t)] = 2^{-2nt} \cdot \text{Diagram} = 2^{-nt} \cdot \text{Diagram} \quad (\text{SM-47})$$

The r.h.s. follows by using unitarity together with the first of (SM-37), and then using the deterministic rule to evolve the initial classical state  $[s_j]_j$  to the classical state  $[s'_j]_j$  on the diagonal. We can now first remove the projectors on the left by continuously applying the r.h.s. of (SM-37), and then by combining unitarity and Eq. (5) the diagram

contracts fully:

$$\text{tr}[\rho_A^n(t)] = 2^{-nt} \dots = 2^{-nt} \underbrace{\dots}_{s'_{2\ell-t+1}} \dots = 2^{-2nt+n} \left( \text{diag} \right)^{t-1} \underbrace{\dots}_{s_{2\ell}}. \quad (\text{SM-48})$$

After noting

$$\underbrace{\text{diag}}_{s_{2\ell}} = 2, \quad (\text{SM-49})$$

we can finally gather all the factors together and obtain

$$\text{tr}[\rho_A^n(t)] = 2^{t(1-n)}. \quad (\text{SM-50})$$

*Region of flat states in a system prepared in the solvable state*

Now we consider a quench from the system prepared in the solvable state everywhere, except for a finite region  $A$  which is initialized in the flat state, and we are interested in the entanglement entropy between  $A$  and the rest at some later time  $t$ . Since the flat state is locally invariant under time-evolution, the transfer matrix factorizes into fixed points for all times  $\ell \leq |A|$  (and not only for  $t \leq \ell/2$ ). What remains to be understood is the intermediate regime with  $\ell < t < 2\ell$ . The trace of the  $n$ -th power of the reduced density matrix is given as

$$\text{tr}[\rho_A^n] = 2^{-2nt} \dots = 2^{n(\ell-2t)} \dots, \quad (\text{SM-51})$$

where the r.h.s. follows by applying unitarity from the top and the local invariance of the flat state. Using now relations (SM-37), we introduce projectors  $\downarrow$  on the left edge and bring them down to the diagonal. Then, using the





we have that the l.h.s. of Eq. (SM-55) is written as

$$\begin{array}{c} \square \\ \diagup \quad \diagdown \\ \square \quad \square \\ \diagdown \quad \diagup \\ \square \end{array} = \frac{1}{2^n} \sum_{\alpha_j=0,1,2,3} \begin{array}{c} \square \\ \diagup \quad \diagdown \\ \square \quad \square \\ \diagdown \quad \diagup \\ \square \end{array}^{\alpha_1, \dots, \alpha_n} = \frac{1}{2^n} \sum_{\alpha_j=0,1} \begin{array}{c} \square \\ \diagup \quad \diagdown \\ \square \quad \square \\ \diagdown \quad \diagup \\ \square \end{array}^{\alpha_1, \dots, \alpha_n}. \quad (\text{SM-60})$$

Next we note that Eq. (SM-59) implies

$$\begin{array}{c} \square \\ \diagup \quad \diagdown \\ \square \quad \square \\ \diagdown \quad \diagup \\ \square \end{array}^{\alpha} = \begin{array}{c} \sigma^{(\alpha)} \\ \downarrow \quad \downarrow \\ \square \quad \square \\ \diagdown \quad \diagup \\ \square \end{array} = \begin{array}{c} \sigma^{(\alpha)} \\ \downarrow \quad \downarrow \\ \square \quad \square \\ \diagdown \quad \diagup \\ \square \end{array}, \quad \alpha = 0, 1. \quad (\text{SM-61})$$

This means that

$$\forall \alpha_j = 0, 1, \quad \begin{array}{c} \square \\ \diagup \quad \diagdown \\ \square \quad \square \\ \diagdown \quad \diagup \\ \square \end{array}^{\alpha_1, \dots, \alpha_n} = \begin{cases} \begin{array}{c} \square \\ \diagup \quad \diagdown \\ \square \quad \square \\ \diagdown \quad \diagup \\ \square \end{array} & \sum_j \alpha_j \text{ even} \\ \begin{array}{c} \square \\ \diagup \quad \diagdown \\ \square \quad \square \\ \diagdown \quad \diagup \\ \square \end{array}_{1,0,\dots,0} & \sum_j \alpha_j \text{ odd} \end{cases}. \quad (\text{SM-62})$$

Plugging back into Eq. (SM-60) we then find

$$\begin{array}{c} \square \\ \diagup \quad \diagdown \\ \square \quad \square \\ \diagdown \quad \diagup \\ \square \end{array} = \sum_{\substack{\alpha_j=0,1 \\ \sum_j \alpha_j \text{ even}}} \begin{array}{c} \square \\ \diagup \quad \diagdown \\ \square \quad \square \\ \diagdown \quad \diagup \\ \square \end{array}^{\alpha_1, \dots, \alpha_n} + \sum_{\substack{\alpha_j=0,1 \\ \sum_j \alpha_j \text{ odd}}} \begin{array}{c} \square \\ \diagup \quad \diagdown \\ \square \quad \square \\ \diagdown \quad \diagup \\ \square \end{array}_{1,0,\dots,0}^{\alpha_1, \dots, \alpha_n}, \quad (\text{SM-63})$$

where we used Eq. (SM-59). Finally, noting

$$\sum_{\substack{\alpha_j=0,1 \\ \sum_j \alpha_j \text{ even}}} \begin{array}{c} \square \\ \diagup \quad \diagdown \\ \square \quad \square \\ \diagdown \quad \diagup \\ \square \end{array}^{\alpha_1, \dots, \alpha_n} = \sum_{\alpha_j=0,1} \begin{array}{c} \square \\ \diagup \quad \diagdown \\ \square \quad \square \\ \diagdown \quad \diagup \\ \square \end{array}^{\alpha_1, \dots, \alpha_n} = \begin{array}{c} \square \\ \diagup \quad \diagdown \\ \square \quad \square \\ \diagdown \quad \diagup \\ \square \end{array}, \quad \sum_{\substack{\alpha_j=0,1 \\ \sum_j \alpha_j \text{ odd}}} \begin{array}{c} \square \\ \diagup \quad \diagdown \\ \square \quad \square \\ \diagdown \quad \diagup \\ \square \end{array}^{\alpha_1, \dots, \alpha_n} = 0, \quad (\text{SM-64})$$

we obtain the r.h.s. of Eq. (SM-55).